BLACK SILICON FABRICATED BY ALUMINIUM-ASSISTED CHEMICAL ETCHING FOR SOLAR CELLS

SHAHNAWAZ UDDIN

UNIVERSITI SAINS MALAYSIA

2023

BLACK SILICON FABRICATED BY ALUMINIUM-ASSISTED CHEMICAL ETCHING FOR SOLAR CELLS

by

SHAHNAWAZ UDDIN

Thesis submitted in fulfilment of the requirements
for the degree of
Doctor of Philosophy

March 2023

ACKNOWLEDGEMENT

Alhamdulillah, a lot of thanks to Allah for providing me a chance to complete my research work successfully. I would like to express my sincere gratitude to my main supervisor, Ts. Dr. Mohd Zamir Pakhuruddin for his valuable and in-depth suggestions, guidance and continuous support throughout this PhD programme. I would also like to thank my co-supervisor, Prof. Md. Roslan Hashim for his kind suggestions and help in this research work. Thanks to Universiti Sains Malaysia (USM), Penang, Malaysia for funding this research work through a short-term grant 304/PFIZIK/6315063.

Much of this work would not have been possible without the technical support from the technical staffs of Nano-Optoelectronics Research (NOR) Laboratory. Some of them to mention are Mrs. Ee Bee Choo, Mr. Abdul Jamil Yusuf and Mr. Yushamdan Yusof. Also thanks to my fellow friends: Dr. Auwal Abdulkadir and others who have given me useful advices and helps during the laboratory works.

Last but not the least, I would like to thank my family members for their motivation, support and patience throughout the whole research work and thesis writing process.

TABLE OF CONTENTS

LIST OF TABLES

Page

LIST OF FIGURES

Page

LIST OF SYMBOLS

ε_f	Free energy of surface of metal film
ε_s	Free energy of surface of substrate
ε_{sf}	Free energy of interface between the substrate and the metal film
γ	Ideality factor (e.g., γ =1 for c-Si)
$\Phi(\lambda)$	Photon flux spectra
η	Power conversion efficiency
λ	Wavelength of light
μ	Micron
μ_e	Electron mobility
μ_h	Hole mobility
ν	Frequency of photon
Ω	Ohm (unit of electrical resistance)
ρ	HF:H_2O_2 ratio ([HF]/([HF] + [H_2O_2]))
^oC	Degree Celsius
A	Absorption or absorptance of light
c	Speed of light in vacuum
d	Film thickness
E_c	Energy of conduction band edge
E_f	Fermi energy or Fermi level
E_{Fn}	Fermi energy level on n-side of a pn-junction
E_{Fp}	Fermi energy level on p-side of a pn-junction
E_g	Bandgap energy
E_{ph}	Energy of photon
E_v	Energy of valence band edge

h	Planck's constant
I	Current
I_D	Diode current
I_{dark}	Current across a pn-junction under dark conditions in forward bias
I_L	Current source
I_{light}	Current across a pn-junction under light illumination (i.e., optical bias)
I_m	Output current available at the maximum power point
I_o	Recombination/reverse-saturation current
I_{ph}	Photocurrent under light illumination
I_{sc}	Short-circuit current
k	Boltzmann's constant
n	Refractive index
N	Light concentration-ratio of PV cell (i.e., number of suns)
N_a	Acceptor concentration
N_d	Donor concentration
n_e	Electron concentration (in cm^{-3})
P_{in}	Input light intensity in mW/cm^2
P_m	Maximum obtainable output electrical power
P_{out}	Output electrical power density in mW/cm^2
P_{SL}	Optical shading loss
q	Electronic charge
R	Reflection of light
$R(\lambda)$	Reflection of light as a function of wavelength
R_{sheet}	Sheet resistance
R_{avg}	Average reflection of light
R_s	Series resistance
R_{sh}	Shunt resistance

S	Spreading-coefficient
$S(\lambda)$	Standard spectral density of photons
T	Absolute temperature in Kelvin
V	Voltage
V_{bi}	Built-in potential barrier in a pn-junction
V_m	Output voltage available at the maximum power point
V_{oc}	Open-circuit voltage
V_T	Thermal voltage (i.e., at room temperature ~26 mV)

LIST OF ABBREVIATIONS

AACE	Aluminium-assisted chemical etching
AFM	Atomic force microscope
Ag	Silver
$AgNO_3$	Silver nitrate
Ag NPs	Silver nanoparticles
Al	Aluminium
AlF_3	Aluminium fluoride
Al_2O_3	Aluminium oxide
AM	Air-mass
AM0	Air-mass outside earth's atmosphere
AM1.5D	Air-mass direct
AM1.5G	Air-mass global equivalent to 1 sun
Ar	Argon
Ar^+	Argon gas ions
ARC	Anti-reflective coating
Au	Gold
B	Boron
b-Si	Black silicon
$C_4H_{10}O$	2-butanol
CB	Conduction band
cm	centimeter
c-Si	Monocrystalline silicon
Cu	Copper
CVD	Chemical vapour deposition
CZ	Czochralski
DC	Direct current
E	Energy
e^-	Electron
EBSD	Electron backscatter diffraction
EDX	Energy dispersive X-ray
e-h	Electron-hole

EQE	External quantum efficiency
F^-	Fluoride ion
FESEM	Field effect scanning electron microscope
FF	Fill factor
GaAs	Gallium arsenide
Ge	Germanium
h^+	Hole
H^+	Hydrogen ion
H_2	Hydrogen
H_2O	Deionized water
H_2O_2	Hydrogen peroxide
H_3O^+	Hydronium ion
H_3PO_4	Phosphoric acid
H_2SiF_6	Hexafluosilicic acid
HCl	Hydrogen chloride acid
HF	Hydrogen fluoride acid
HNO_3	Nitric acid
HV	High vacuum
Hz	Hertz (unit of frequency)
InP	Indium phosphide
IQE	Internal quantum efficiency
IR	Infrared
I-V	Current-Voltage
J-V	Current density-Voltage
k	Kilo
K	Kelvin (unit of absolute temperature)
KOH	Potassium hydroxide
L	Liter (unit of volume)
LCD	Liquid crystal display
LED	Light emitting diode
m	Milli
M	Mega
mc-Si	Multicrystalline silicon
ml	Milliliter

mm	Millimeter
nm	Nanometer
N_2	Nitrogen
$NaAlO_2$	Sodium aluminate
NaOH	Sodium hydroxide
Ni	Nickel
Ni-NPs	Nickel nanoparticles
NOR lab	Nano-optoelectronics research laboratory
NPs	Nanoparticles
p	Pico (i.e., 10^{-12})
P	Phosphorus
P_2O_5	Phosphorus pentoxide
$(P_2O_5)_x (SiO_2)_{1-x}$	Phosphosilicate glass
Pd	Palladium
PFD	Photon flux density
PSi	Porous silicon
PSL	Porous silicon layer
Pt	Platinum
PV	Photovoltaic
PVD	Physical vapour deposition
RCA	Radio Corporation of America
RF	Radio frequency
RIE	Reactive ion etching
RMS	Root mean square
rpm	Revolution per minute
sccm	Standard cubic centimeter per minute
SCR	Space charge region
SE	Stain etching
SEM	Scanning electron microscope
Si	Silicon
Si_3N_4	Silicon nitride
SiC	Silicon carbide
SiNHs	Silicon nanoholes
SiNWs	Silicon nanowires

SiN_x	Silicon nitride
SiO_2	Silicon dioxide
SRH	Shockley Read Hall
SRV	Surface recombination velocity
STC	Standard test condition
STEM	Scanning transmission electron microscopy
t	Time
TCO	Transparent conductive oxide
USA	United States of America
USD	United States Dollar
USM	Universiti Sains Malaysia
UV	Ultraviolet
UV-Vis-NIR	Ultraviolet-Visible-Near infrared
V	Volt (unit of potential difference)
VB	Valence band
W	Watt (unit of power)
ZnO	Zinc oxide

LIST OF APPENDICES

SILIKON HITAM DIFABRIKASI OLEH PUNARAN KIMIA BERBANTU ALUMINIUM UNTUK SEL SURIA

ABSTRAK

Dalam penyelidikan ini, pemangkin aluminium (Al) digunakan untuk memfabrikasi silikon hitam nanoliang b-Si melalui proses yang baru dibangunkan, dipanggil punaran kimia berbantukan aluminium (AACE). Dalam proses ini, filem nipis pemangkin Al (12-30 nm) dimendapkan pada wafer monohabluran (c-Si) jenis p (100) diikuti dengan penyepuhlindapan haba yang cepat (250-450 oC) selama 40 minit dalam persekitaran nitrogen. Wafer kemudiannya dipunar pada suhu bilik (~25 oC) untuk tempoh masa yang berbeza (10-60 minit) dalam larutan asid hidrofluorik (HF), hidrogen peroksida (H_2O_2) dan air ternyahion (H_2O) untuk menghasilkan b-Si nanoliang. Semasa proses AACE, pelbagai parameter telah dikaji termasuk ketebalan pemangkin Al, suhu penyepuhlindapan, masa punaran dan komposisi kimia larutan HF-H_2O_2-H_2O. Sifat morfologi, optik dan elektrik permukaan b-Si nanoliang telah dikaji menggunakan mikroskop elektron pengimbasan pelepasan medan (FESEM), mikroskop daya atom (AFM), spektrofotometer UV-Vis-NIR dan sistem pengukuran kesam Hall. Wafer c-Si planar menunjukkan pantulan purata wajaran (R_{avg}) sekitar 40% dalam julat panjang gelombang 300-1100 nm dan mobiliti lubang (μ_h) 235 cm^2/V-s. Daripada proses AACE yang optimum, R_{avg} terendah sebanyak 5.7% dicapai daripada b-Si nanoliang yang dihasilkan dengan menggunakan ketebalan mangkin Al 24 nm, penyepuhlindapan terma pada 400 oC selama 40 minit dan punaran dalam HF-H_2O_2-H_2O (10-1-10 ml) larutan selama 30 minit. B-Si nanoliang yang dioptimumkan mempamerkan kedalaman purata 436 nm, diameter purata 31 nm, liputan permukaan 45%, punca min kuasa dua kekasaran (RMS) 36 nm dan μ_h 147 cm^2/V-s. Untuk

fabrikasi sel PV, pemancar jenis-n akan diresapkan pada 950 oC selama 22 minit ke dalam c-Si p-jenis (untuk rujukan) dan berpemukaan rata b-Si nanoliang. Sel PV dicirikan oleh simulator suria diod pemancar cahaya putih (LED) pada suhu bilik (~25 oC) dengan kuasa pencahayaan input 45 mW/cm^2. Sel PV c-Si planar menunjukkan, ketumpatan arus litar pintas (J_{sc}) 13 mA/cm^2, voltan litar terbuka (V_{oc}) 454 mV, faktor isian (FF) 55% dan kecekapan penukaran (η_{avg}) 6.93%. Manakala sel PV b-Si nanoliang yang optimum mempamerkan, J_{sc} 27 mA/cm^2, V_{oc} sebanyak 510 mV, FF 61% dan η_{avg} sebanyak 18.62%. Peningkatan sel PV b-Si adalah disebabkan oleh penyerapan cahaya jalur lebar yang dipertingkatkan dalam penyerap b-Si nanoliang.

BLACK SILICON FABRICATED BY ALUMINIUM-ASSISTED CHEMICAL ETCHING FOR SOLAR CELLS

ABSTRACT

In this research, aluminium (Al) catalyst is used to fabricate nanoporous black silicon (b-Si) via a newly developed process, called aluminium-assisted chemical etching (AACE). Al as catalyst having a low diffusivity (0.94 cm^2/s) slows down the etching rate in the AACE process for a **better control over the morphology of nanopores and makes the AACE process low-cost too**. In this process, a thin film of Al catalyst (12-30 nm) is deposited on p-type (100) monocrystalline (c-Si) wafers followed by thermal annealing (250-450 ^oC) for 40 minutes in a nitrogen atmosphere. The wafers are then etched at room temperature (~25 ^oC) for different time durations (10-60 minutes) in a mixed solution of hydrofluoric (HF) acid, hydrogen peroxide (H_2O_2) and deionized water (H_2O) to produce nanoporous b-Si. During the AACE process, various influencing parameters have been investigated including Al catalyst thickness, annealing temperature, etching time and chemical composition of HF-H_2O_2-H_2O solution. Surface morphological, optical and electrical properties of the nanoporous b-Si have been studied using field emission scanning electron microscope (FESEM), atomic force microscope (AFM), UV-Vis-NIR spectrophotometer and Hall effect measurement system. Planar c-Si wafer demonstrates weighted average reflection (R_{avg}) of around 40% within 300-1100 nm wavelength region and hole mobility (μ_h) of 235 $cm^2/V\text{-}s$. From the optimized AACE process, the lowest R_{avg} of 5.7% is achieved from the nanoporous b-Si produced by using Al catalyst thickness of 24 nm, thermal annealing at 400 ^oC for 40 minutes and etching in HF-H_2O_2-H_2O (10-1-10 ml) solution for 30 minutes. The optimized nanoporous b-Si exhibits nanopores

with an average depth of 436 nm, an average diameter of 31 nm, surface coverage of 45%, root mean square (RMS) roughness of 36 nm and μ_h of 147 cm^2/V-s. For the fabrication of photovoltaic (PV) cells, an n-type emitter is diffused at 950 ^oC for 22 minutes into the planar p-type c-Si (for a reference) and nanoporous b-Si samples. The PV cells are characterized by a white light emitting diode (LED) solar simulator at room temperature (~25 ^oC) with an input illumination power of 45 mW/cm^2. The planar c-Si PV cell demonstrates short-circuit current density (J_{sc}) of 13 mA/cm^2, open-circuit voltage (V_{oc}) of 454 mV, fill factor (FF) of 55% and an average conversion efficiency (η_{avg}) of 6.93%. On the other hand, the optimized nanoporous b-Si PV cell exhibits J_{sc} of 27 mA/cm^2, V_{oc} of 510 mV, FF of 61% and η_{avg} of 18.62%. The improved efficiency of the b-Si PV cell is attributed to the enhanced broadband light absorption in the nanoporous b-Si absorber.

CHAPTER 1

INTRODUCTION

1.1 Introduction

In today's world, out of various renewable clean energy sources, the electrical power production by photovoltaic (PV) cells is increasing day by day. The PV cells convert the light energy directly into electrical energy by the photovoltaic effect observed for the first time in 1839 by Edmond Becquerel, a French scientist [1]. The output electrical power from a PV cell is governed by how efficiently a PV cell works. Therefore, to meet a greater demand for a clean power generation and compete with the conventional (fossil fuels) and other renewable energy sources, the PV cells should have higher efficiencies. The incumbent and new PV technologies are setting up new milestones for power conversion efficiencies as shown in the world record PV cell efficiencies chart of Figure 1.1 [2]. The continued research efforts have expanded the global production of PV cells based on silicon and other thin-film technology; they are generating clean energy more than 821 TWh globally by the end of 2021. Like the previous years (2019, 2020 and 2021), the market share of silicon and other thin-film PV technologies is expected to be maintain at 95% and 5% respectively in the current year (2022) [3,4]. The dominance of silicon-based PV industry is due to abundance of silica, stability, environment friendly, economy of scale and technology maturity, thanks to the advancements in microelectronics and nanoelectronics [5]. Moreover, increased efficiency (~26%) and reduced cost (~$0.24/Watt) of silicon PV cells are facilitating to dominate the PV industry [6].

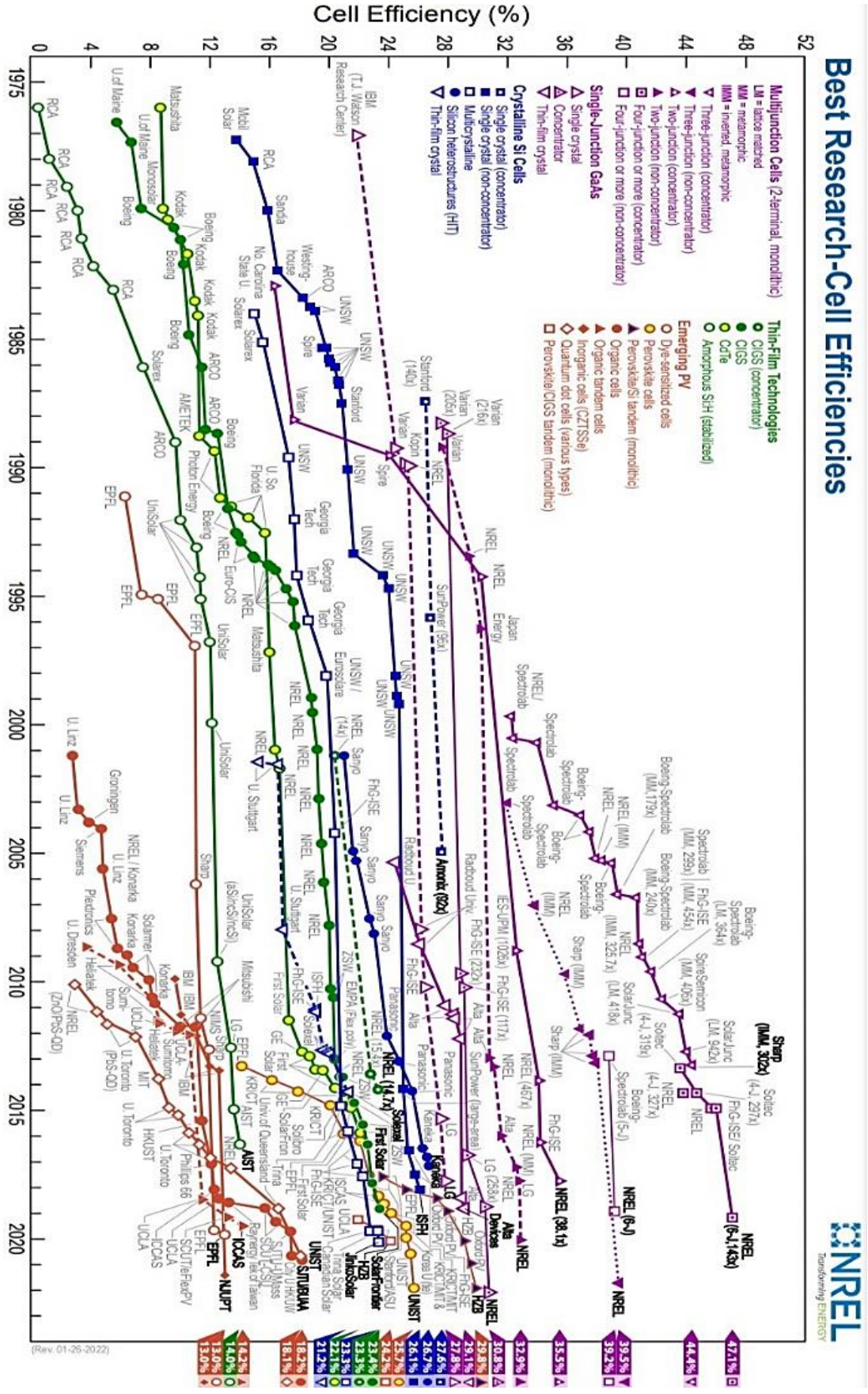

Figure 1.1 World record PV cell efficiencies. A courtesy of the National Renewable Energy Laboratory (NREL), USA [2].

Nevertheless, the monocrystalline silicon (c-Si) material in its original form suffers from poor absorption of incident light (~60%) in a wideband (300-1100 nm) wavelength range because of low absorption coefficient (3105 cm^{-1} at $\lambda = 633$ nm) and due to the indirect bandgap, which attributes to relatively poor light absorption in the near infrared region [7,8]. The poor absorption of the incident light reduces the power conversion efficiency of the PV cells. Besides the high reflection, the efficiency of the c-Si PV cells should be enhanced by adopting a mechanism to modify the surface of the planar c-Si to trap/couple the incident light within the c-Si material so that it absorbs a wideband of light energy to the maximum extent (> 90%). In literature, various techniques have been used to texture the top surface of the planar c-Si by generating micro-/nano-structures [9]. The micro-/nano-structures created on the surface of planar c-Si behave like a graded refractive index layers and trap or couple the incident light very effectively [10,11]. Some of the surface texturing techniques of planar silicon include Mazur's method (laser treatment method) [12], reactive ion etching (RIE) [13], stain etching [14], FFC Cambridge process (electrochemical reduction method) [15], electrochemical etching [16] and metal-assisted chemical etching (MACE) [17]. The employed technique to texture the surface of planar c-Si should be facile and have an excellent control over the morphology of the fabricated micro-/nano-structures along with providing good optical and electrical characteristics. Among all these techniques, MACE is considered the most facile, the most economical, quick, versatile, reproducible, controllable and scalable [17,18,19,20]. As shown in Figure 1.2, the modified top surface of planar c-Si may have micro-structures (with dimensions greater than the wavelength of light) or nano-structures structures (with dimensions less than the wavelength of light) or hybrid-structures (a combination of micro- and nano-structures) [21].

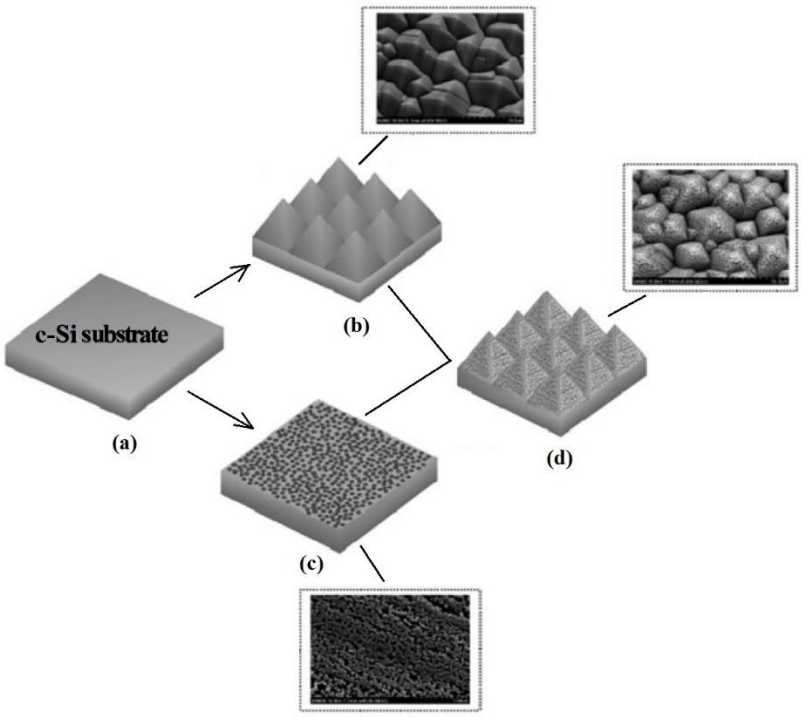

Figure 1.2 (a) Planar c-Si substrate (b) Micro-structured pyramids (c) Nano-structured pyramids (d) Hybrid micro-/nano-structured pyramids [21].

1.2 Background of black silicon

Black silicon (b-Si) is a crystalline silicon (c-Si) surface with an array of nanotextures with superior broadband light absorption from ultraviolet (UV) to infrared (IR) regions [22]. For the first time in 1995, b-Si was developed by Jansen et al. using RIE method resulting in micro-spikes on the top surface of c-Si [23]. The b-Si has a very low reflection of incident wideband light or absorbs the incident light much efficiently and appears black to the naked eyes as shown in Figure 1.3 [24,25]. The superior light absorption in b-Si owes to the enhanced light trapping/coupling because of the graded refractive index at air-silicon interface attributed by the nanostructures with smaller dimensions as compared to the wavelength of incident light [24]. Having a strong wideband (300-1100 nm) light absorption characteristic and low cost of fabrication, b-Si is investigated as a potential replacement for planar c-Si in many applications (e.g., photovoltaics, photodetectors, etc.) [24,26,27,28].

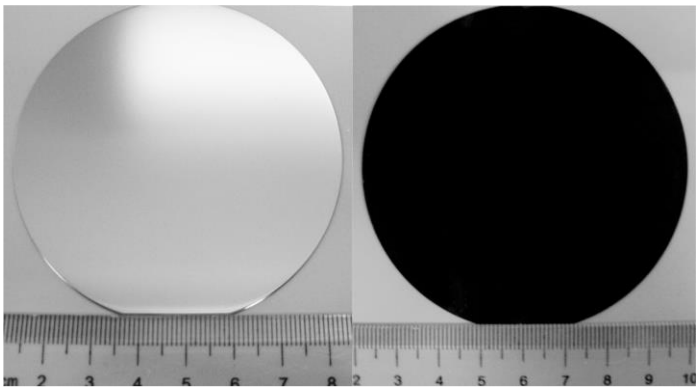

Figure 1.3 The planar c-Si and b-Si wafers [25].

1.3 Applications of black silicon

To achieve the excellent light trapping/coupling in the nanostructures on the surface of the b-Si, various shapes such as nanowires [11], nanopillars [29], nanocones [30], nanopores [31] and nanograss [32] have been fabricated by the researchers. It should be noted that no standard rules are applied in naming the shape of the fabricated nanostructures. It is just a visual interpretation, and hence some names are interchangeably used for similar shapes [33]. Other than the excellent broadband light absorption property, the b-Si has many other superior properties such as surface hydrophobicity, antibacterial surface, high aspect-ratio and modified band structure. Therefore, with excellent properties, the b-Si is a potential choice for a range of desirable applications such as PV cells [24,26], photodetectors [27,28], energy storage devices [36], biosensors [37], self-cleaning [38], antibacterial-surfaces [39], drug-analysis [40], terahertz-emitters [41] and photoluminance [42], etc. Nevertheless, in comparison to the fragile and delicate free-standing silicon nanowires/nanopillars, the silicon nanoholes or nanopores (SiNHs or SiNPs) are mechanically robust and exhibit extremely low wideband light reflection property owing to effective light trapping/coupling in the nanohole/nanopore arrays which are the accrued advantages with nanoporous b-Si [34,35]. Therefore, in this research work, the nanoporous b-Si

has been studied and explored to devise a method to fabricate it easily and economically with a fine control over the morphology of the nanopores for the PV applications.

Owing to its excellent wideband light absorption or anti-reflection characteristic, b-Si material may be an ideal choice for silicon-based PV cells with a better performance in terms of cost to power conversion efficiency ratio since the b-Si solar cells do not necessarily need an anti-reflective coating (ARC) resulting in a lower manufacturing cost [24]. However, the major challenge with the use of the b-Si in PV cells is enhanced surface recombinations of charge carriers (photogenerated electron-hole pairs) in the large surface area of the nanostructures resulting in a low power conversion efficiency [24]. This problem in b-Si PV cells is solved by passivating the top surface of the nanotextured b-Si by growing or depositing a thin layer of a passivating material such as silicon oxide (SiO_x), silicon nitride (SiN_x) and aluminium oxide (Al_2O_3) [24,43,44,45]. The nanoporous b-Si solar cells have reported a high efficiency of 18.2% without any ARC [46] and 22.1% with a passivating layer of Al_2O_3 acting as ARC as well [24]. A solar panel manufacture from China, Solarspace Technology, produces solar panels (model :12BB) based on polycrystalline black silicon which demonstrates an efficiency of ~21.5% [47].

1.4 Motivation for nanoporous b-Si PV cells

The silicon wafer-based technology dominates (~95%) of PV industry due to the abundance of silica (SiO_2) in earth's crust, its stability in various environments, the matured fabrication technology and the constant reduction in the technology cost [3,4,48]. This is despite the poor absorption of light in the planar c-Si (~60%), owing to its low absorption coefficient (3105 cm^{-1} at $\lambda = 633$ nm) and indirect bandgap energy

(1.12 eV) [8,49,50]. Numerous efforts are underway to improve light absorption in c-Si which is vital to increase photocurrent in PV cells. Use of quarter-wavelength thick layer of the dielectric material (such as SiO_x, SiN_x, Al_2O_3, ZnO, or a combination of these) as an ARC is one of the most common PV industry standards to reduce the reflection (below 10%) from the planar c-Si surface [24,51,52].

Another promising, cost-effective and less-stringent approach to reduce the broadband light reflection is by incorporating nanotextures on planar c-Si surface (i.e., nanostructured b-Si) resulting in an average light reflection even below 5% without any ARC. This enhanced light trapping in the nanotextured surface of the planar c-Si is due to the refractive index grading effect, i.e., the incident light is trapped in the nanostructures smaller in dimensions as compared to wavelength which have a graded-refractive index across their thickness (at least half-wavelength of the incident light) [53,54,55,56]. Moreover, the nanostructured b-Si provides wideband (300-1100 nm) absorption and anti-reflective property over a wider angle as compared to an ARC [55,57]. It should be noted here that the trapping of light takes place when the incident light enters the medium with a graded refractive index due to either nanostructures or microstructures and the optimum trapping of light in visible range is achieved if the depth/height of nanostructures/microstructures is 250 nm or more [58,59]. Nevertheless, the nanostructured b-Si suffers from more surface recombination of charge carriers associated mainly with high surface area of nanostructures on planar c-Si but can be reduced by using a passivation layer of any of the commonly used dielectric material, such as SiO_x, SiN_x or Al_2O_3 [24,55].

1.5 Problem statement

The MACE process is the most used technique to texture the surface of the planar c-Si to enhance the broadband light absorption (>90%) which in turn increases the photocurrent, leading to the higher efficiency PV cells [60]. In this process, the average height/depth, average diameter, surface coverage (i.e., density of nanostructures) and distribution of the nanostructures can be controlled by catalyst thickness [64], annealing temperature [65], etching time [66] and chemical composition of the etching solution [66,67]. But a rapid etching rate in MACE process due to the higher diffusivities of the commonly employed metal catalysts such as Ag (1.61 cm^2/s), Au (1.27 cm^2/s) and Cu (1.15 cm^2/s), limits a fine control over the morphology of the nanostructures [68]. A high value of diffusivity of a metal catalyst helps in the quick transport of holes to the metal-silicon interface leading to faster oxidation of silicon and its etching by HF. Additionally, owing to a strong stability of commonly used metal catalysts (e.g., Ag, Au and Cu) in the etching solution, there is an extra step to remove the residues of these metal NPs from the surface of b-Si after etching process since they do not dissolve during the MACE process. Furthermore, the noble metal catalysts (e.g., Ag, Au, etc.) are expensive which render the MACE a costly process.

Therefore, all the above factors open new opportunities for other metals (which have a lower diffusivity, consumable during the etching process and have a lower cost), to be evaluated as a potential catalyst for the MACE process. Aluminium (Al) is one of the promising alternative metal catalysts for this purpose because Al has relatively low diffusivity (0.94 cm^2/s), very reactive towards HF (the etching agent), low-cost and technology-friendly (currently being used in c-Si PV cell manufacturing process as a rear metal contact) [24,68,69,70,71]. Thus, employing Al in the MACE

process in place of a noble metal catalyst, provides a fine control over the morphology of the nanostructures due to slow etching rate attributed to its lower diffusivity. Additionally, the dissolution of Al in the etching solution of HF-H_2O_2-H_2O, stops the etching process or regulates the synthesis of shallower nanopores. Al as a catalyst also reduces the cost of MACE process. To date, no such work has been carried out to evaluate Al as a potential catalyst in MACE process to fabricate nanoporous b-Si for PV cell applications.

Hence, here in this research work, a novel MACE process which utilizes Al as the catalyst is developed, via a process called aluminium assisted chemical etching (AACE). In this process, a thin layer of Al catalyst (12-30 nm) is deposited on c-Si substrate by the direct current sputtering process followed by the thermal annealing (250-450 ^oC) in nitrogen (N_2) ambient (with a flow rate of 2.0 L/minute) for solid-state dewetting the Al film. The solid-state dewetting process produces a random array of nanoholes into the Al catalyst film and makes it porous too. After that, the c-Si with an array of nanoholes on top surface is etched in an aqueous solution (10 ml of H_2O) containing HF (1-10 ml) and H_2O_2 (1-10 ml) at the room temperature (~25 ^oC) for a varying time (10-60 minutes), resulting in nanoporous b-Si. The surface morphology, optical properties and electrical properties of the nanoporous b-Si are characterized in comparison to planar c-Si.

For the fabrication of PV cells, a pn-homojunction is formed by diffusion of phosphorus at 950 ^oC for 22 minutes. The morphological, optical and electrical characterizations of the fabricated pn-homojunction are performed. Later, pn-homojunction PV cells are developed by depositing a front Ag grid contact and an Al back contact with around 300 nm thickness. The co-firing of the metal contacts is done

in at 600 ^{o}C for 22 minutes to complete the planar c-Si/nanoporous b-Si PV cells. The PV cells are characterized using solar simulator (for I-V curve) and other parameters for their performance evaluation in comparison to planar c-Si PV cells.

1.6 Objectives

The main objectives of the research are as the following:

1. To investigate the surface morphological, optical and electrical properties of nanoporous b-Si synthesized by aluminium-assisted chemical etching (AACE) process.

2. To optimize AACE process by evaluating Al catalyst thickness, annealing temperature, etching time and chemical composition of etching solution to produce a nanoporous b-Si with $R_{avg} < 10\%$.

3. To evaluate the performance of nanoporous b-Si PV cells in comparison to the planar c-Si PV cell.

1.7 Thesis outline

The present thesis contains six chapters presented as follows:

Chapter 1 briefly introduces b-Si and its applications in various fields. It mainly focuses on the need and use of b-Si for PV cell, problem statement, research objectives and outline of the thesis.

Chapter 2 includes detailed theory related to fabrication of b-Si via MACE process and PV cell. It also explains the concepts of the solar spectrum, PV effect, light trapping in b-Si and solid-state dewetting process. A brief description of literature review of fabrication methods of b-Si/PV cells is included at the end of the chapter.

Chapter 3 outlines the fabrication of nanoporous b-Si via AACE process, process flow for fabrication of nanoporous b-Si, equipments and procedures used for the synthesis of nanoporous b-Si and the fabrication of the nanoporous b-Si PV cells. Firstly, it explains the chemistry involved in the fabrication of nanoporous b-Si via AACE process. Secondly, it outlines the steps (process flow) involved in the fabrication of the optimized nanoporous b-Si and PV cells. It explains briefly about the basic principles involved in the equipments used for cutting, deposition, thermal annealing and characterization or measurement during the development of nanoporous b-Si and PV cells.

Chapter 4 presents and discusses the experimental results, the effects of varying different parameters during the synthesis of nanoporous b-Si and PV cells, the characterization results, possible mechanisms involved and the explanation of findings at different stages of the fabrication process. It also presents the optimum conditions for the synthesis of the best samples of the nanoporous b-Si and PV cells based on them.

Chapter 5 concludes the experimental findings, presents original contributions in this research work and recommends future works in the same area.

CHAPTER 2

THEORETICAL BACKGROUND AND LITERATURE REVIEW

2.1 Introduction

In PV industry, c-Si dominates the annual solar cell production. This owes to constant improvement in solar cell efficiency, reducing technology cost, proven long-term stability and economies of scale [5,9]. In planar c-Si, the absorption of incident light is relatively poor due to its indirect bandgap and low absorption coefficient (3105 cm^{-1} at λ = 633 nm) [7,8,72]. Low absorption of light results in a lower value of J_{sc} in planar c-Si PV cells. To mitigate this issue, various approaches have been investigated. One of the promising approaches involves fabrication of nanotextures on the front surface of the planar c-Si resulting in b-Si [10]. With the nanotextures on the top surface of b-Si, the broadband (300-1100 nm) average reflection can be reduced <10% because of incident light coupling/trapping in the graded refractive index medium created by the nanotextures. As a result, the b-Si exhibits superior light absorption well above 90% within wideband (300-1100 nm) wavelength range, which is vital for PV conversion application [10].

2.2 Solar spectrum

To harvest the abundant and clean energy from the sun, the PV cells have attracted a considerable interest in recent decades because of direct conversion from sunlight to electricity and simplicity of their installation [73]. The input power to the PV cells comes from the sun in the form of photons with varying wavelengths whose intensities depend on different parameters: such as location on earth, atmospheric conditions, day of the year and time of the day [74]. The photons with a wavelength (λ), having energy equal to or greater than the bandgap energy (E_g) of the material used in

the PV cell (i.e., $E_{ph} \geq E_g$ or $hc/\lambda \geq E_g$), can activate the electron-hole pairs to generate electricity. Thus, in case of c-Si (E_g = 1.12 eV) based single-junction PV cell, useful $\lambda \leq 1110$ nm out of the whole solar spectrum and the theoretical maximum power conversion efficiency is ~30% (Shockley-Quisser limit) under AM1.5G (1 sun, i.e., 1000 W/m^2 or 100 mW/cm^2) [73]. Typically, the solar irradiance measures the power of incident photons and represented in the standard units of W/m^2.

The standards for solar light irradiance are set by American Society for Testing Materials (ASTM), e.g., on earth-surface, air-mass global (AM1.5G or 1 sun) (which includes direct and diffuse radiations) corresponds to ~1000 W/m^2; AM1.5D (only includes direct radiations) corresponds to ~888 W/m^2 (approximately 10% lower than AM1.5G) and the standard outside earth's atmosphere or extra-terrestrial AM0 corresponds to ~1360 W/m^2 (approximately 36% higher than AM1.5G) [74,75,76]. The standardization of solar spectra is necessary for the comparative study of PV cells' performance, even in a laboratory where solar simulators can be used to duplicate the standard solar spectra. The solar spectrum of the solar irradiance for AM0/AM1.5G/AM1.5D is plotted in Figure 2.1. For the assessment of the performance of a PV cell, the photon flux, $\Phi(\lambda)$, is commonly used to evaluate total input incident light power density (P_{in}) in Equation (2.1) assuming optimally one electron-hole pair is generated per incident-photon (ideally no optical or recombination losses occur, i.e., EQE=1) [74].

$$P_{in} = \int \frac{hc}{\lambda} \Phi(\lambda)\, d\lambda \qquad 2.1$$

where Planck's constant, h = 6.626×10^{-34} J-s, and speed of light in vacuum, c = 3×10^8 m/s.

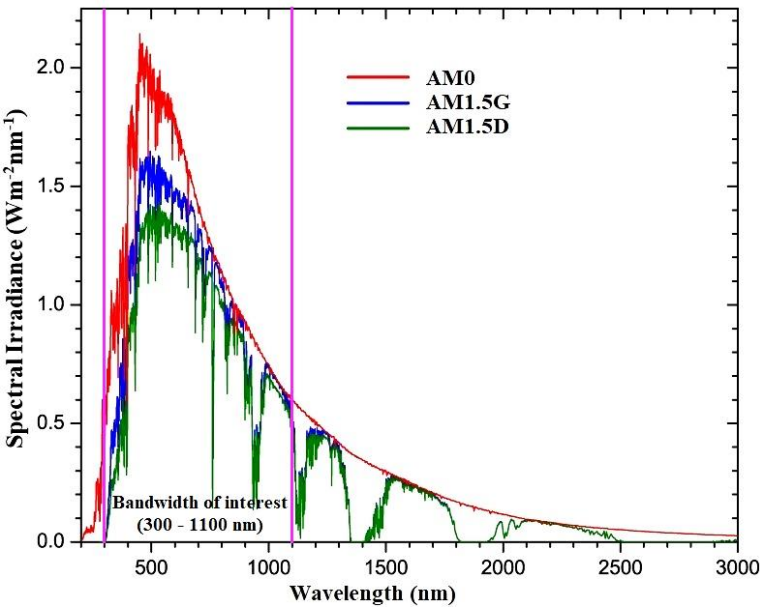

Figure 2.1 The spectral irradiance of sunlight [76].

The schematic diagram of a nanoporous b-Si PV cell, its equivalent circuit and I-V characteristic of a single PV cell are illustrated in Figures 2.2(a-c) respectively. The extreme cases of the current and voltage are represented by short-circuit current (I_{sc}, i.e., zero-voltage current across the load) and open-circuit voltage (V_{oc}, i.e., zero-current voltage across the load) respectively. Practically, the bandgap of the absorber material of the PV cells puts upper bounds on the values of V_{oc} and I_{sc} (i.e., $V_{oc} \leq E_g$ and I_{sc} reduces with increase in E_g) [74,77]. The I_m and V_m in the I-V characteristics of the PV cell represent the current and voltage when the PV cell produces the maximum output power (P_m) or the point of maximum power conversion efficiency.

The output electrical power density (P_{out}) in W/cm^2 produced by the PV cell with a top surface area (A) in response to incident input solar power (P_{in}) can be calculated by the following Equation (2.2).

$$P_{out} = \frac{I}{A} \times V = J \times V \qquad 2.2$$

where J = I/A measured in A/cm^2 is the current density produced by the PV cell.

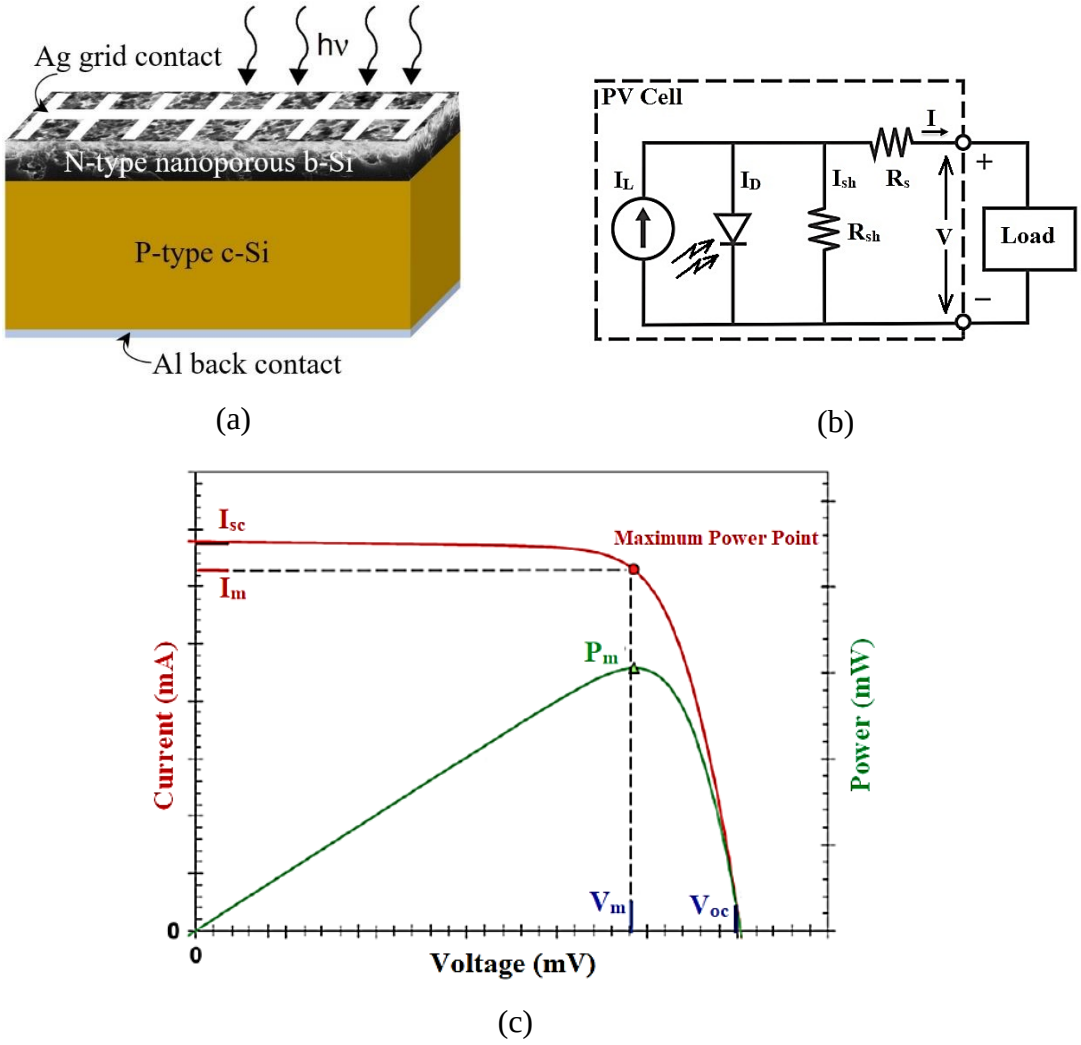

Figure 2.2 (a) A schematic diagram of a nanoporous b-Si PV cell under normal light illumination (b) The equivalent circuit of the PV cell under normal light illumination [74] (c) The current-voltage (I-V) characteristics of the PV cell under light illumination [74].

One of the promising routes to enhance the quantum efficiency of the single junction PV cell is to enhance the incident light absorption by the material of which the cell made of. This enhancement in the absorption by the b-Si material will increase the quantum efficiencies and which will result in high power conversion efficiency as explained in the following paragraphs.

External quantum efficiency (EQE) of a PV cell is a measure of the output current produced when the solar light of a particular wavelength illuminates on the cell.

The integration of EQE over the whole solar electromagnetic spectrum gives the maximum current density ($J_{sc\,(max)}$) as evaluated by the following Equation (2.3) [11,78].

$$J_{sc\,(max)} = q \int EQE(\lambda)\, S(\lambda)\, d\lambda \qquad 2.3$$

where q is the electronic charge (1.6 x 10^{-19} C) and S(λ) is the standard spectral photon density under the standard AM1.5 solar spectrum (1000 W/m^2 at ~25 ^{o}C).

In other words, EQE is defined as the ratio of total number of charge carriers collected at the electrodes of the PV cell to the total number of photons of a particular wavelength incident on the cell, which is given by the following Equation (2.4) [79]:

$$EQE = \frac{Electrons/second}{Incident\ photons/second}$$

$$or \quad EQE = \frac{(Current)/(Charge\ of\ one\ electron)}{(Total\ power\ of\ photons)/(Energy\ of\ one\ photon)} \qquad 2.4$$

Another type of quantum efficiency, i.e., internal quantum efficiency (IQE) is defined as the ratio of total number of charge carriers collected at the electrodes of the PV cell to the total number of photons of a particular wavelength absorbed by the cell, which is given by the following Equation (2.5) [80]:

$$IQE = \frac{Electrons/sec}{Absorbed\ photons/sec} = \frac{EQE}{(1 - Reflection)} \qquad 2.5$$

It has been observed that for a practical PV cell having non-zero reflection of light, IQE is always greater than EQE.

The power conversion efficiency (η) of the PV cell is given as the ratio of maximum output electrical power (P_m) to the incident solar illumination power (P_{in}) and is determined by the following Equation (2.6) [81]:

$$\eta = \frac{P_m}{P_{in}} = \frac{J_m \times V_m}{P_{in}} = \frac{J_{sc}\ V_{oc}\ FF}{P_{in}} \quad 2.6$$

where J_m and V_m represent the current-density and voltage at a point of maximum power conversion of the PV cell, J_{sc} is the short circuit output current density, V_{oc} is the open circuit output voltage, FF is the fill factor that is defined as the ratio of maximum obtainable electrical power from the PV cell to the product of J_{sc} and V_{oc} [82], i.e.,

$$FF = \frac{(P_{obtainable})_{max}}{J_{sc}\ V_{oc}} = \frac{J_m \times V_m}{J_{sc} \times V_{oc}} \quad 2.7$$

Therefore, by definition, FF≤1 that can be observed from Equation (2.7). In an ideal condition (when no power is extracted from the PV cell), the power generated per square area would be equal to $V_{oc} \times J_{sc}$, but because of various losses (e.g., recombination loss, heating loss and shading loss, etc.), the maximum obtainable power density, $P_m = V_m \times J_m = FF \times V_{oc} \times J_{sc}$ [81].

2.3 Photovoltaic effect

As shown in Figure 2.3, the photons of incident light may get absorbed in a semiconductor (such as c-Si) and generate electron-hole pairs if the energy of the absorbed photons (hν) is greater than or equal to bandgap energy (E_g) of the semiconductor (i.e., $h\nu \geq E_g$) [77,81]. In other words, this process creates an effective positive (h^+)/negative (e^-) charge in the valence/conduction band of a semiconductor. In a normal semiconductor, these photogenerated electrons in excited state drop back to their ground state by recombining with holes in the valence band. The recombination of these e^--h^+ pairs results in emission of light in the form of photons (i.e., radiative recombination) or heat in the form of phonons (i.e., non-radiative recombination) [81].

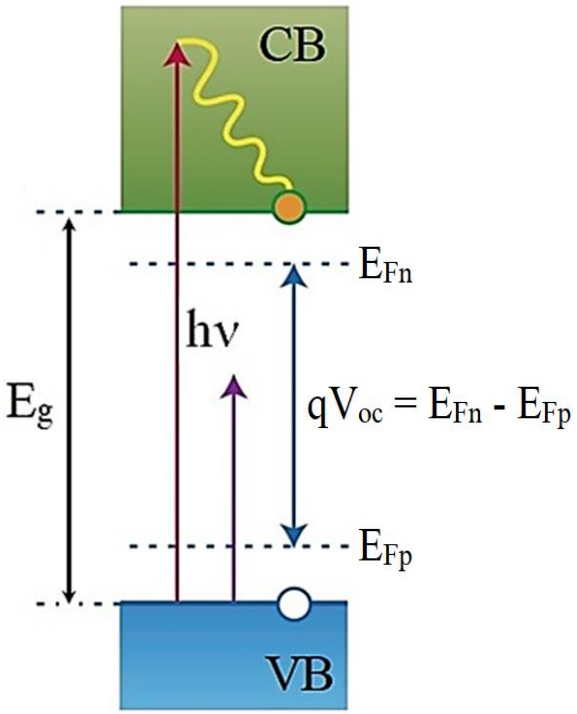

Figure 2.3 Energy band diagram of a single junction PV cell showing generation of e^--h^+ pair under incident light illumination. Photon with an energy below E_g is not absorbed [77].

The PV effect or a net flow of photogenerated e^- across the material in the form of photocurrent takes place when an asymmetric potential or charge separation is created on the end terminals (electrical contacts). An asymmetric potential in a single piece of c-Si is established by doping the opposite surfaces of c-Si wafer by p-type (e.g., boron) and n-type (e.g., phosphorus) impurities respectively. An alternative method is by doping the already boron-doped (p-type) c-Si by phosphorus, i.e., by creating a pn-homojunction in c-Si material. Thus, the built-in field generated due to asymmetric potential in a good PV material separates the charge carriers efficiently for a better rectification and photovoltaic action. In other words, the photogenerated charge carriers should be collected by the respective electrodes with a minimum number of recombinations [81].

The overall performance of a PV cell is characterized by its electrical parameters (such as V_{oc}, I_{sc}, FF, and η) [81,83,84]. It is well known fact that $V_{oc} \leq E_g$ and I_{sc} reduces

with increase in E_g. Therefore, as permitted by thermodynamics, a maximum permissible efficiency of ~30% is possible for the PV cell fabricated by using an absorber material with E_g = 1.1 eV [74,85].

The efficiency of an operating PV cell is limited by various kinds of losses occurring inside/outside the device [80]. The charge carriers may recombine directly from valence band to conduction band or through the localized trap-states in the forbidden-band (or bandgap) caused by the imperfections in the crystal. Energetically, both kinds of charges (e^- and h^+) get trapped and recombine with the opposite kind of charge carriers. In a conventional semiconductor, majority of trap-states are localized in the bandgap of surfaces' atoms because of the presence of under-coordinated atoms. A thin layer of a passivating material can be deposited to reduce the surface-effect by completing the coordination with under-coordinated atoms at surface while no participation in conduction of charge carriers. The direct recombination of charge carries from band to band can be minimized by improving the mobility of charge carriers and separating the charge carriers with an electric field [81].

2.4 Working principle of a PV cell

As shown in Figure 2.4, the solar cell uses PV effect to convert the solar energy into electricity (direct current) [86]. In other words, the incident photons of light having energy ($h\nu$) equal to or more than the bandgap energy (E_g) of the semiconductor material of the solar cell, generate electron-hole pairs and subsequently the built-in electric field helps in separating these photo-generated charge carriers at two terminals (anode and cathode) to develop DC current in the device.

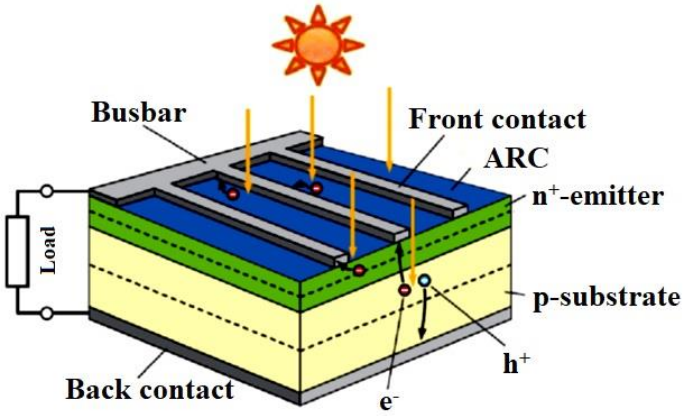

Figure 2.4 A schematic diagram of a conventional solar cell [83].

The PV cells having pn-junction formed on the c-Si are the oldest and the most popular one. A PV cell is just a simple pn-junction diode formed by putting the p-type and n-type semiconductors in direct contact with each other. A homojunction PV cell is developed by bringing together the p-type and n-type regions/layers of same semiconductor material as illustrated in Figure 2.5(a) [87]. When the p-type and n-type c-Si materials come in contact of each other, the majority charge carriers (h^+ in p-type and e^- in n-type) diffuse from one side to another and neutralize each other to create a space charge region (SCR) with a net electric-field in the junction space [87]. During the diffusion of charge carriers (e^- and h^+), the Fermi levels of p-type and n-type silicon are aligned and an energy barrier ($qV_{bi} = E_{Fn}–E_{Fp}$) is developed which should be surmounted by e^-/h^+ to cross from n-/p-side to p-/n-side as shown in Figure 2.5(b) [87]. An external applied voltage (at least 67% of bandgap energy in amplitude) can decrease/increase this energy barrier to operate the pn-junction in forward/reverse bias mode or to allow/stop the current to flow which is a rectification action [87]. Under the dark conditions, the current (I_{dark}) starts to rise at knee point in the forward-bias operation of pn-junction while in the reverse bias mode, the current remains zero as shown in I-V curve of Figure 2.5(d) which is given by the following Equation (2.8) [87].

$$I_{dark} = I_o\left(e^{\frac{V}{\gamma V_T}} - 1\right) \qquad 2.8$$

where I_o is a reverse saturation current through the pn-junction diode, γ is the ideality factor of the diode (γ = 1 for c-Si diode), V_T = kT/q is the thermal equivalent voltage, k is the Boltzmann constant (1.38×10^{-23} J/K), T is the absolute temperature, q is the electronic charge (1.6×10^{-19} C). At room temperature (i.e., T=300 K), V_T = ~26 mV.

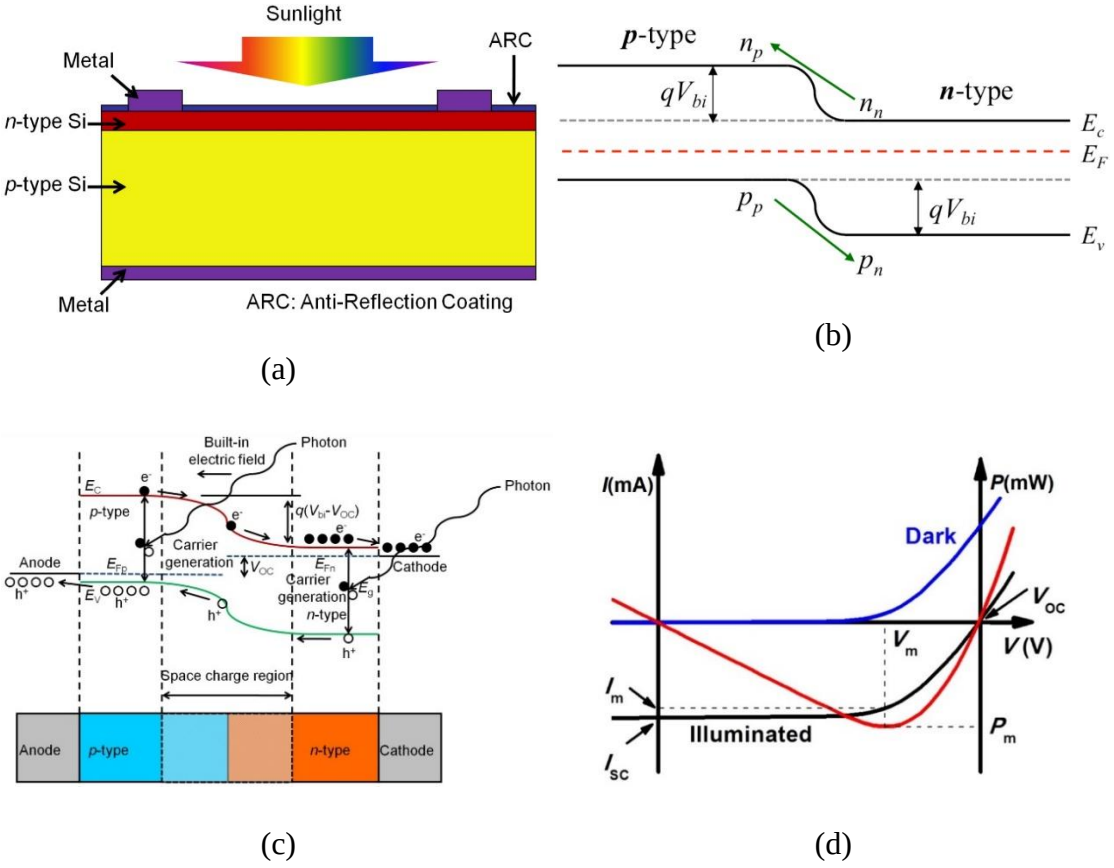

Figure 2.5 (a) A schematic of c-Si pn-junction PV cell (b) The energy band diagram of a pn-junction PV cell under dark condition (c) The energy band diagram a pn-junction PV cell under light illumination (d) I-V and power curves of pn-junction PV cell under dark and light-illumination [87].

Under light illumination, the energy band diagram of pn-junction PV cell is modified slightly with open circuit condition as illustrated in Figure 2.5(c). The photons in the incident light having the energy (i.e., hν ≥ E_g) gets absorbed and excite the

electrons from valence band of p-/n-type side to the conduction band of the respective sides resulting in generation of e^--h^+ pairs (i.e., photogenerated charge carriers) [81]. In this way, the e^-/h^+ generated in p-/n-type regions represent minority charge carriers which can diffuse and cross over to other side and reduce the built-in potential barrier if their lifetime is long enough to travel the SCR [87]. When sufficient light is illuminated (i.e., optical bias) and no load connected across the terminals, an open-circuit voltage (V_{oc}) is developed between the terminals of the pn-junction PV cell (i.e., $V_{oc} = E_{Fn} - E_{Fp}$) [87]. A direct current starts to flow between the anode and cathode terminals if they are short-circuited or connected through an external circuit as shown in Figure 2.5(d) which is given by the following Equation (2.9) [87].

$$I_{light} = I_{dark} - I_{ph} = I_o\left(e^{\frac{V}{\gamma V_T}} - 1\right) - I_{sc} \tag{2.9}$$

where I_{ph} is the photocurrent or short-circuit current (i.e., anode and cathode are short-circuited), i.e., $I_{ph} = I_{sc}$. Under open-circuit condition (i.e., $V = V_{oc}$), the current across the pn-junction PV cell is reduced to zero (i.e., $I_{light} = 0$). Thus, from Equation (2.9),

$$0 = I_o\left(e^{\frac{V_{oc}}{\gamma V_T}} - 1\right) - I_{sc}$$

$$\Rightarrow V_{oc} = \gamma V_T \, ln\left(\frac{I_{sc}}{I_o} + 1\right) \tag{2.10}$$

The output power from the pn-junction PV cell can be calculated by just multiplying the current and voltage at the point of operation ($P_{out} = I \times V$) as shown in Figure 2.5(d) [87].

2.5 Light trapping in black silicon

The planar and polished surface of c-Si contribute to approximately 40% reflection of incident light in 300-1100 wavelength range which results in a lower value of J_{sc} in the planar c-Si PV cells [10]. To mitigate this issue, micro-/nano-structures (with dimensions comparable to the incident light) are created on the c-Si surface resulting in b-Si [10]. With the textured surface of b-Si in the form of nanopores or micropores or mixture of them, the broadband average reflection can be reduced (<10%) because of graded refractive index phenomenon observed in the micro-/nano-pores [7].

The reflection behaviour of the incident light from different surfaces (planar and textured) of c-Si is shown in Figures 2.6(a-d) which is self-explanatory. As the nanostructures on the surface increase (i.e., a combination of micro- and nano-pores), the incident light gets coupled more because of multiple reflections, refractions and transmissions which extend the optical pathlength [31]. Thus, the micro- and nano-scale pores on the surface of b-Si enhance the absorption of photons significantly through the trapped light owing to their geometry optical effect and graded index effect which give the reflected light multiple chances to enter the material and favour the light coupling [31]. Ultimately, by texturing the top polished surface of the planar c-Si through ordered or random micro-/nano-pores, the average light absorption is enhanced in a broad wavelength range (300-1100 nm) [31].

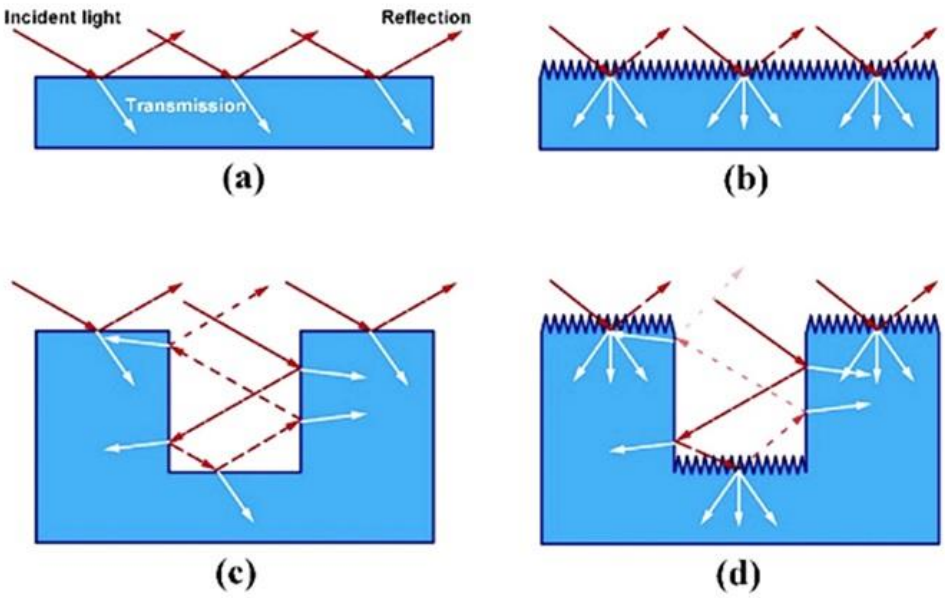

Figure 2.6 A schematic of reflection and propagation of incident light through c-Si surface with varying structural features: (a) Planar surface (b) Nanoporous surface (c) Microporous surface (d) Micro-/nano-porous surface [31].

As illustrated in Figure 2.7, the incident light is trapped in an inhomogeneous medium with a graded refractive index (n) in the form of nanoporous b-Si on the surface of the planar c-Si substrate which acts as a light trapping medium and as an antireflective layer too. As illustrated in the figure, the maximum light is trapped inside the nanoporous b-Si due to multiple refractions and scattering of light if optimum values of the average depth (d), surface coverage and porosity (i.e., graded refractive index, n) of nanopores are achieved [88,89]. The transmittance through a 280 µm thick planar c-Si substrate (an opaque material) is assumed to be zero, thus, only light reflection and absorption takes place within the as-fabricated nanoporous b-Si and c-Si substrate as well.